**ORIGINAL ARTICLE**

# Experimental study and machining parameter optimization on powder-mixed EDM of Nimonic 901 using feed-forward backpropagation neural networks

**Ravi Varma Penmetsa[1] · Ashok Kumar Ilanko[2] · Siriyala Rajesh[3] · Rama Bhadri Raju Chekuri[3]**

## Abstract

The earliest and most widely utilized procedure of unconventional machining is referred to as electric discharge machining (EDM), which is a process of non-contact machining for eliminating the material from the workpiece (i.e. electrically conductive) with the usage of electric discharge series. This article proposes an experimental investigation and optimal selection of input process parameters involved in powder-mixed EDM (PM-EDM) process of a workpiece made of Nimonic 901 alloy with an electrode of copper-tungsten (Cu–W). In addition, silicon carbide (SiC) is used as a powder particle due to its more resistance to mechanical steadiness at greater temperatures, high hardness, exceptional thermal conductivity, low coefficient of thermal expansion, corrosion and oxidation etc. The impact of input process variables like concentration of mixed powder $(C_p)$, servo voltage $(V_s)$, peak current $(I_p)$ and pulse-on-time $(T_{on})$ on output response features assessed in terms of tool wear rate (TWR), surface roughness (SR) and material removal rate (MRR) was also examined. Furthermore, the Taguchi design approach with $L_{18}$ orthogonal array is employed to find the optimal combination of process parameters using the analysis of signal-to-noise $(S/N)$ ratio. Furthermore, back-propagated neural network (BPNN) with feed-forward (FF) architecture is utilised to determine the approximate solutions and best fit for the optimization and search issues. Finally, the findings of the experimental MRR (E-MRR) confirmation test are compared to the MRR values derived using FF-BPNN model, i.e. P-MRR. Similarly, the experimental SR (E-SR) and experimental TWR (E-TWR) results were also compared to the SR and TWR computed utilizing FF-BPNN model, i.e. P-SR and P-TWR, respectively.

**Keywords** Electric discharge machining · Powder mixing · Nimonic 901 alloy · Optimization · Taguchi approach · Artificial neural networks

✉ Ravi Varma Penmetsa
  ravivarma.mechengg@gmail.com

  Ashok Kumar Ilanko
  akrt02au@gmail.com

  Siriyala Rajesh
  rajeshsiri.mech@gmail.com

  Rama Bhadri Raju Chekuri
  bhadri.mech@gmail.com

[1] Department of Manufacturing Engineering, Annamalai University, Annamalai Nagar, Chidambaram, Tamil Nadu, India

[2] Department of Mechanical Engineering, Government College of Engineering, Bargur, Tamil Nadu, India

[3] Deprtment of Mechanical Engineering, Sagi Rama Krishnam Raju Engineering College, Bhimavaram, Andhra Pradesh, India

## 1 Introduction

It is not possible to achieve the engineering materials' machining with the conventional machining process owing to the increased enhancement of properties in such materials. The quality of tool should be much harder than the workpiece in the traditional process of machining [1]. The barriers of material machining are the produced damage and the expense of tool materials while using the materials. The shapes of machine are hardly progressive; micromachined components and intricate design with high quality of surface are needed along with novel materials. These parts are unable to produce viably using the traditional machining processes. To fulfil these requirements, new processes have been improved. In different industries like automobile, aircraft and tool and die making, these methods are being distinguished. Based on the indications of triggering to material expulsion from workpiece, the grouping of non-conventional machining processes has been performed

accordingly [2, 3]. Therefore, it is required to choose the appropriate method for an application carefully with the exploitation of different non-conventional machining techniques effectively [4, 5]. Electric discharge machining (EDM) is one type of electro-thermal machining and non-conventional technique, which refers to the spark eroding or spark machining process. In aviation and other mechanical applications, it has been utilized for machining high-quality temperature-safe materials and hard materials like titanium and super combinations of solidified steels [6]. For creating electrical sparks, the required space is obtained by the electrical energy in the manufacturing process, and the removal of material is occurred due to the spark's thermal energy [7]. In general, the EDM tool is referred to as the negative terminal and the workpiece refers to the positive terminal. The potential differentiation connects between workpiece and tool. The input parameters like dielectric medium, polarity, the gap between tool and workpiece, time pulse, maximum current, external flushing through the spark gap, maximum current, working voltage and open circuit voltage have influenced the EDM performance. For machining of temperature-safe, superior quality and hard-to-machine alloys, EDM is used as a fundamental thermal process that requires arranging of a plasma channel between the workpiece and the device. In the mould making and die industries, these materials have been used the most [8]. The EDM process has been exploited in aerospace equipment manufacturing, for instance, in engine, landing gear, impeller and fuel system, where high stress and temperature requirements prevail. Because of poor integrity of surface, the life and safety of components have been questioned. The problem of poor surface integrity that has been raised has been addressed by the PM-EDM application rather than the conventional EDM. In automobile industry, some applications included the piston heads, cylinder liners, carburettors and engine block manufacturing.

## 1.1 Principle of PM-EDM

For dispensing with the EDM procedure inconveniences and upgrading EDM limit, the PM-EDM has considered as one of the imaginative and advanced procedures over the last couple of decades [9]. Figure 1 shows the principle of PM-EDM, which is used for increasing the material removal rate (MRR) and reducing surface roughness (SR) contrary to EDM based on gap increment between the workpiece and electrode. The crisscross pattern is carried out if voltage applies to the powder particles that become invigorated [10]. Because of electric field, the charged particles have been improved, and they are considered as the conductors for promoting the breakdown of gap. The spark gap has increased between the workpiece and the tool. The particles have come closer to each other and are arranged in a structured way under the sparking area. In the current flow direction, the interlocking is occurred between the powder particles. These structures can be useful to bridge the gap between electrodes. The short circuit is resulted with the reduction of dielectric fluid's insulating strength due to the bridging effect. The series discharge and earlier explosion of the gap are caused in the electrode area. The faster erosion is caused from the surface of the workpiece by the rapid sparking in discharge, and it increased the MRR. The rough machining efficiency is improved by implementing the PM-EDM, which improved the machining efficiency by 70% compared to the powder-free dielectric EDM. It has achieved the machined SR [11].

In the dielectric oil, the particles of fine powder are suspended in PM-EDM. If enough voltage of 80 to 320 V is supplied among these particles, then the electric field will be generated in the inter-electrode gap. The ionization of dielectric has been performed for the conventional EDM. On the powder particles' top and bottom, the positive and negative charges have been accumulated under the applied electric field respectively. Here, the positive charge is the workpiece, and the negative charge is the tool. The powder particles' chains have been formed by the electrodes' capacitive effect. The primary breakdown of discharge is occurred, where the highest electric field density is included between '$b$' and '$a$' as shown in Fig. 2. Between two powder particles, such as an electrode and a powder particle, this breakdown may occur (workpiece or tool). After collecting electric charges at '$c$' and '$d$' and the first discharge, the electric charges are redistributed. Further discharge is

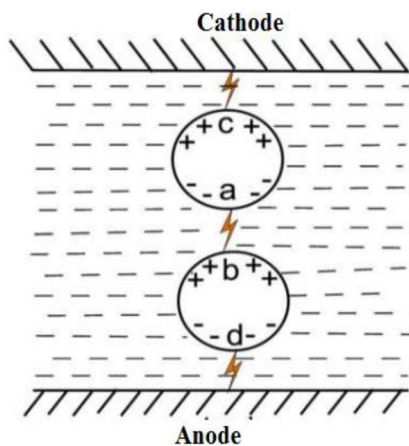

**Fig. 1** PM-EDM process schematic
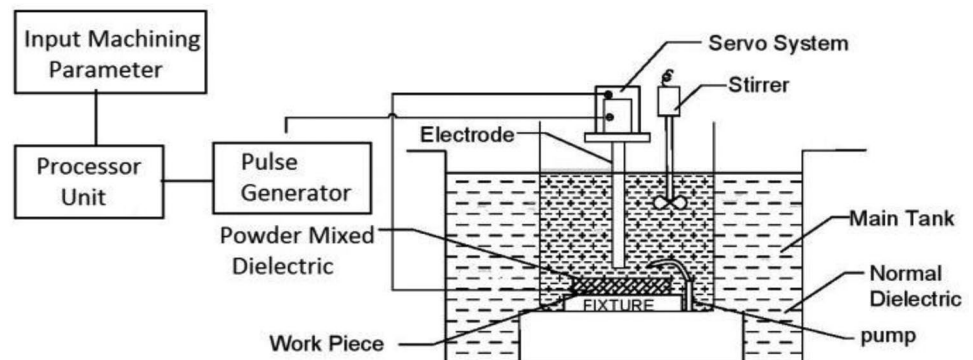
**Fig. 2** Series discharging in PM-EDM

occurred between the powdered and other particles, which includes the higher electric field density [12, 13].

## 1.2 Discharge gap expansion

The discharge gap size relies on the powdered particle properties, i.e. both electrical and physical. The overall resistance of dielectric is mitigated by the free electrons that are present in the conductive powder particles under the conditions of high temperature. From a longer distance, the spark is to be generated with the increased conductivity, and the discharge gap is enlarged [14, 15].

**Fig. 3** Different forces acting on a powder particle
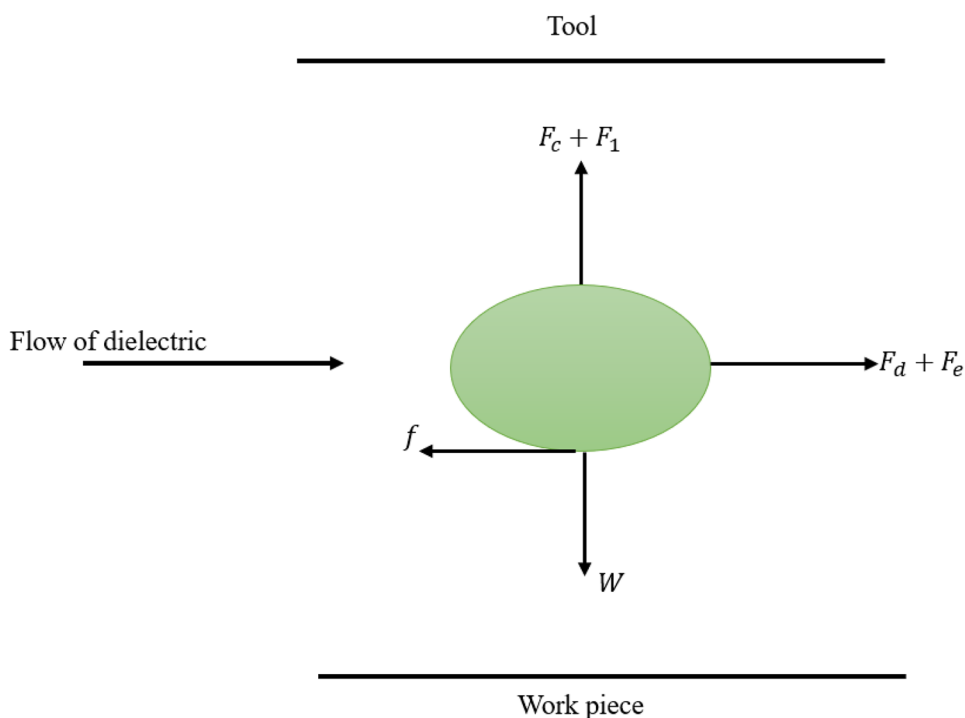
### 1.2.1 Multiple discharges

In PM-EDM, multiple discharge paths have been observed because of the zigzag rapid movements of the adjourned powder particles. The uniform distribution of energy is assured, and the numerous craters are formed in the time of single pulse. Significantly, the discharge of PM-EDM is different compared to the input pulse unlike traditional EDM. Because of multiple discharges, the voltage is fluctuated rapidly within the duration of single pulse [16, 17].

## 1.3 Influence of powder characteristics

Jahan et al. [18] presents the analytical model for PM-EDM with comprehensive study. Figure 3 shows different forces with schematic representation impacting the powder particle in the gap of the inter-electrode. Here, $f$, $F_e$, $F_d$, $F_c$ and $F_l$ are friction, electric, drag, columbic and lift forces, respectively, and $W$ indicates the particle's self-weight.

The formula derived by the powder-mixed dielectric's breakdown energy is given in Eq. (1):

$$E_{br}^2 = E_i^2 - 2\sigma T \frac{1}{\varepsilon_1}\left(\frac{\varepsilon_p + 2\varepsilon_1}{\varepsilon_p - \varepsilon_1}\right)\left[\frac{1}{r^3}\left(\ln \frac{N_f}{N_i}\right)\right] \tag{1}$$

where the initial voltage for concentration $N_i$ is denoted as $E_i$; the voltage for final concentration $N_f$ is denoted with $E_{br}$; $\sigma$ is referred to as the constant of Boltzmann; temperature is denoted with $T$; dielectric permittivity and powder particle permittivity are referred to as $\varepsilon_1$ and $\varepsilon_p$, respectively; and the

powder particle radius is represented as $r$. It is evident from Eq. (1) that the values of $E_{br}$ rely on the radius of powder particle, the change in concentration ($N$), and the values of $\varepsilon_1$ and $\varepsilon_p$, respectively.

The main novelty and contribution of this work is as follows:

- Considering the Nimonic alloy 901 as a workpiece, which has higher strength of yield and creep resistance at 1110 °F temperatures, i.e. 600 °C. In addition, it has a substantial amount of iron content that enables it to unify the strength with the features of good devising
- The addition of powder mixing in the dielectric fluid of EDM, which enhances its conductive strength and distance of spark gap between the workpiece and the tool
- Implementation of Taguchi design approach for finding the optimal combination of input process parameters like $C_p$, $I_p$, $V_s$ and $T_{on}$ for the enhanced output response parameters like SR, tool wear rate (TWR) and MRR
- Implementation of ANN for optimization of process parameters in PM-EDM using FF-BPNN model

## 2 Related work

Many researchers have examined the experimentations of PM-EDM with different kinds of materials as workpiece and electrode tools. The influence of EDM's input parameters such as $T_{on}$, $T_{off}$, $I_p$ and voltage on output metrics like SR, MRR and TWR in the stationary tool without the dielectric power mix and rotary tool with dielectric EDM powder mix is investigated [19]. The major effecting parameter is $T_{on}$, which significantly influenced both TWR and MRR. In [20], the authors used silicon powder floating plus kerosene as dielectric for exploring these dielectrics' effect on the performance criteria, such as MRR and SR in the titanium combination machining (Ti-6A1-4 V). To implement the PM-EDM regarding SR and MRR, the parameters for the methodology have been chosen as the powder included into the EDM dielectric liquid, $T_{off}$, $T_{on}$ and $I_p$. The lower SR and higher MRR have been obtained by the high concentration and high $I_p$. In [21], the authors have addressed the Taguchi technique with the application in integration with the method for order of preference in like the grey relational analysis and the ideal solution for evaluating the optimization of various features for performance in PM-EDM H-11 die steel utilizing the copper electrode. The influence of procedure parameters, for instance $T_{on}$, duty cycle, $V_g$, $C_p$ and $I_p$, on different response parameters like SR, EWR, TWR and MRR has been studied by mixing the chromium powder into the dielectric fluid. Here, the conductive powder into dielectric fluid with less defects, cracks and small SR is improved by the surface topography that is related to the crater size

and the recast layer's distribution on the surface. In [22], the authors studied the impact of graphite powder concentration on dielectric fluid that is considered as drinking water to machine the electric discharge of Ti-6A1-4 V alloy. To provide the features of MRR and SR, Taguchi approach is exploited to obtain the parameters for EDM, including graphite's $C_p$, $T_{on}$, $I_p$ and $T_{off}$. The impact of parameters on the performance was also investigated. The SR and MRR have increased with $I_p$ increment and increased by increment of powder concentration, and MRR was reduced less significantly. The experimental studies of SiC microparticle suspended dielectric effect on machining of Ti-6A14V with the electrode of tungsten carbide are examined in [23]. In dielectric, the parameters of major electric discharge milling process effects are included in the powder concentration, capacitance and voltage effects on responses, like TWR and MRR. At lower levels of powder concentration, minimum TWR was observed and increased with voltage and capacitance. Singh et al. [24] presented the experimental investigations of TWR in the aluminium 6061 alloy PM-EDM reinforced with the particles of 10% silicon carbide (AA6061/10%SiCp composite). The process of mechanical stir casting fabricated the composite material, and EDS and SEM were characterized further. In the dielectric fluid, the tungsten powder was mixed with concentration of 4 g/l. With the increasing of current, TWR is increased significantly. A moderate reduction in tool wear rate, gap voltage ($V_g$), $T_{off}$ and $T_{on}$ is resulted due to huge $T_{on}$. The PM-EDM approach is used that reduces the tool wear rate of 51.12% compared with the basic process of EDM.

Surekha et al. [25] validated the Inconel 825 machinability when adding the graphene nanopowder for the EDM's die sinking dielectric fluid. Based on the surface response approach, the conditions of optimum process have been built. The most affecting parameters are $T_{on}$, $V_g$ and $I_p$ over SR, TWR and MRR. Opoz et al. [26] investigated EN31 and high-carbon hot die steel (H13) and tungsten-copper and two electrode graphite materials (more than 99% purity) (0.014% Ti, 0.047% Z, 0.121%Ni, 19.462% Cu, 79.36% W) of diameter 20 mm. The electrode material chemical composition and workpiece have been estimated before the experimentation on an optical emission spectrometer DV-6. For machining of surface, the grinding of each workpiece has been performed. Different parameters with their effects were concluded, and the size of input current crater was increased on the machined surface. If the surface was machined with copper powder in the dielectric fluid, the uniform distribution of particle on the surface with fewer microcracks is observed. Selvarajan et al. [27] explored the effect of metrics such as powder concentration, powder type and powder concentration on the workpiece of EN-19. To assess the experimental results, the Taguchi methodology was also adopted with three levels and seven factors based on the orthogonal array

**Table 1** Nimonic alloy 901 chemical compositions

| Element | Weight % |
|---|---|
| Titanium | 2.9 |
| Chromium | 12.5 |
| Manganese | 0.5 max |
| Cobalt | 1.0 max |
| Nickel | 42.5 |
| Molybdenum | 5.75 |
| Iron | Balance |
| Sulphur | 0.03 max |
| Carbon | 0.1 max |
| Silicon | 0.4 max |
| Aluminium | 0.35 max |
| Copper | 0.5 max |

**Table 3** Chemical composition of SiC

| Parameter | Value |
|---|---|
| Thermal conductivity | 3 W m K |
| Molecular weight/molar mass | 40.11 g/mol |
| Specific heat | 1800 j/kg K |
| Point of melting | 2,730 °C |
| Density | 3.21 g/cm$^3$ |

of $L_9$. It is significant the effect of powder concentration and achieved larger MRR. Firstly, TWR is increased, and then, it is reduced with increment of $T_{on}$ and $I_p$. Choudhury et al. [28] verified the material of Ti-6A1-4 V-ELI with PM-EDM to determine the effects of SiC powder concentration on surface topography, structures and particle deposition. The mechanism of material transfer improved by low pulse currents and greater suspended particle concentration based on the analysis of the results. The process of current material transfer is depleted at a very high pulse due to the scarcity of secondary discharges. In [29], the authors examined the demanded industrial composite materials with EDM and the impact of varying metrics on the performance of process.

Chaudhury et al. [30] have investigated the method of hybrid PM-EDM based on multi-walled and aluminium powders of carbon nanotube that were combined with kerosene for machining the alloy steel of EN19 with brass electrode. The aluminium powder was added to EDM to machine the alloy steel of EN-19 based on a brass electrode as studied in [31]. The values of $I_p$ and $V_g$ impacted the MRR based on the experimental results. Panda and Kumar [32] enhanced AISI D3 (HCHCr die steel type) surface hardness using the process of PM-EDM with the assumption of manganese powder mixing in distinct densities (i.e. 5 g/l, 10 g/l and 15 g/l) in the oil of dielectric. In addition, a technique of the experimental design was also employed for examining the process' variable impact on the output response parameter known as hardness of surface. Recently, there have been a couple of works that addressed the systematic and methodological review of PM-EDM [33, 34]. Ilani and Khoshnevisan studied the PM-EDM with an electrode tool

**Table 2** Composition properties of Cu–W

| Composition | Density (g/cm$^3$) | Resistivity (μΩ cm) | Hardness (Kgf /mm$^2$) |
|---|---|---|---|
| W50/Cu50 | 11.85 | 3.2 | 115 |

of acrylonitrile butadiene styrene which is coated with a copper metal–based thin layer [35]. Additionally, the fused deposition modelling method of rapid prototyping is utilized for enhancing the electrode tool conductivity for the PM-EDM and MRR, TWR, and SR have been measured w.r.t. the process arguments like $I_p$, $T_{on}$, and $C_p$ of aluminium powder. In addition, recently, fuzzy-based networks [36], ANNs [37, 38] and multi-objective optimization using meta-heuristic optimization techniques like the whale optimization algorithm with cuckoo search [39] have been developed, which are used for optimizing the data.

However, none of the literatures addressed the effectiveness of Nimonic alloy 901 as a workpiece material with Cu–W as electrode material. The Nimonic alloy 901 has



**Fig. 4** Machining process of PM-EDM

**Table 4** Input process parameters with their corresponding levels

| Parameter | Level 1 | Level 2 | Level 3 | Level 4 | Level 5 | Level 6 |
|---|---|---|---|---|---|---|
| $C_p(\%)$ | 0 | 4 | 6 | 8 | 10 | 12 |
| $T_{on}(\mu s)$ | 10 | 15 | 20 | | | |
| $I_p(A)$ | 5 | 10 | 15 | | | |
| $V_s(V)$ | 4 | 5 | 6 | | | |

higher strength of yield and creep resistance at 1110 °F temperatures, i.e. 600 °C. In addition, it has a substantial amount of iron content that enables it to unify the strength with the features of good devising. Moreover, the addition of powder mixing in the dielectric fluid of EDM enhances its conductive strength and distance of spark gap between the workpiece and the tool. Therefore, this article proposes the experimental investigation and optimization of process parameters in PM-EDM of Nimonic alloy 901 workpiece materials, with Cu–W electrode. Furthermore, the Taguchi design approach was also employed for finding the optimal combination of input process parameters like $C_p$, $I_p$, $V_s$ and $T_{on}$ for enhanced output response parameters like SR, TWR and MRR.

## 3 Materials and methods

In this work, the material of Nimonic alloy 901 is used as a workpiece with thickness of 4 mm and dimensions of $60 \times 35$ mm. The age of Hardenable Ni–Fe-Cr super alloy is the Nimonic alloy 901 (UNS N09901/W.Nr. 2.4662) with the addition of aluminium, titanium and molybdenum. According to the specifications of a customer and final application, the alloying route includes the combinations of vacuum arc re-melting, electro slag re-melting and vacuum induction melting. For shafts, gas turbine engine discs, casings, rings and sealing with the maximum temperature of 600 °C, the alloy is used. Cu–W electrode material is made up of a mixture of tungsten and copper, with discrete particles of one metal interspersed in a matrix of another, as copper and tungsten are not solvable in each other. It is 10 mm in diameter and 21.5 mm in length. The material qualities and

**Table 5** Experimental conditions

| Working conditions | Description |
|---|---|
| Workpiece | Nimonic 901 alloy ($60 \times 35 \times 4$ mm) |
| Electrode | Copper-tungsten (diameter of 10 mm and length of 21.5 mm) |
| Machining time | 5 min |
| Gap voltage | 70 V |
| Polarity | Normal |
| Dielectric | SiC powder |

chemical compositions of the electrodes and workpiece are shown in Tables 1 and 2, respectively.

Mechanical steadiness at greater temperatures, high hardness, exceptional thermal conductivity, low coefficient of thermal expansion, corrosion, and oxidation are only a few of the physical–chemical features of SiC powder. Table 3 presents the chemical compositions of SiC.

### 3.1 Performance measurements

SR, MRR and TWR are used as the output performance measurements. Here, the value of surface finish is yielded through the measurement of mean absolute deviation from average surface level based on the computer-controlled tester of SR. TWR is referred to as the electrode material removal of volumetric percentage tool.

The machining performance is better with the smaller TWR in PM-EDM. The better performance is achieved using TWR with lower features. Based on the below equation, it can be estimated:

$$\text{TWR} = \frac{T_b - T_a}{t} \times 1000 \, \text{mg/min} \tag{2}$$

$T_b$ refers to the tool weight before machining, and $T_a$ denotes the the tool weight after machining.

MRR is determined based on the material volume removed per unit time and is used as the key parameter impacting the process time of machining and productivity. MRR is defined as the ratio between the difference of the workpiece in the post and pre machining weight and the workpiece density and machining time. The expression of MRR is formulated as follows:

$$\text{MRR} = \frac{W_b - W_a}{\rho_w \times t} \times 1000 \, \text{mm}^3/\text{min} \tag{3}$$

where the weight of workpiece is denoted as $W_a$ and $W_b$ for after and before machining, respectively (in g); $t$ represents

**Table 6** Considered criteria for the type of response with their corresponding response name

| Response name | Response type |
|---|---|
| MRR | HB |
| SR | LB |
| TWR | LB |

the processing time of machining and $\rho_w$ denotes the workpiece material density. Nimonic 901 alloy density is 8140 kg/m$^3$, and machining time is 5 min.

## 3.2 Design of experiments using Taguchi method

The design of experiments approach was used to collect data and produce accurate results in this study. For orthogonal array ($L_{18}$), four process parameters were chosen: $I_p$ (A), $T_{on}$ (μs), $C_p$ (%) and $V_s$ (V), and the results were evaluated utilizing MINITAB 19 software. First, the cutting process is utilized to attain the required shape and size of both the workpiece and electrode. Then, measure the workpiece weight before the process of machining. Now, the output values are monitored on the screen after feeding the chosen

input process parameters to the machine. Finally, the process of PM-EDM will be terminated after completion of the entire process and then the same will be iterated for the next sample.

## 4 Experimentation setup

The experiments have been carried out for studying the impacts of one or more process parameters on the whole machined surface with good quality of finishing. The major objective of the project is to estimate the impact of $C_p$, $T_{on}$, $V_s$ and $I_p$ on the output response characteristics such as MRR, TWR and SR during the machining of Nimonic901 alloy using the process of PM-EDM as shown in Fig. 4. The

**Table 7** Obtained values of output response features such as MRR, SR and TWR

| S. no | $C_p$(%) | $T_{on}$(μs) | $I_p$(A) | $V_s$(V) | MRR (mm$^3$/min) | SR (μm) | TWR (mg/min) |
|---|---|---|---|---|---|---|---|
| 1 | 0 | 10 | 5 | 4 | 2.241 | 3.123 | 0.04 |
| 2 | 0 | 15 | 10 | 5 | 2.713 | 2.546 | 0.035 |
| 3 | 0 | 20 | 15 | 6 | 4.998 | 5.452 | 0.033 |
| 4 | 4 | 10 | 5 | 5 | 2.321 | 2.652 | 0.03 |
| 5 | 4 | 15 | 10 | 6 | 4.459 | 2.761 | 0.031 |
| 6 | 4 | 20 | 15 | 4 | 4.012 | 5.003 | 0.022 |
| 7 | 6 | 10 | 10 | 4 | 3.985 | 2.245 | 0.029 |
| 8 | 6 | 15 | 15 | 5 | 4.864 | 3.768 | 0.021 |
| 9 | 6 | 20 | 5 | 6 | 5.831 | 3.690 | 0.036 |
| 10 | 8 | 10 | 15 | 6 | 4.039 | 2.612 | 0.028 |
| 11 | 8 | 15 | 5 | 4 | 3.195 | 3.389 | 0.034 |
| 12 | 8 | 20 | 10 | 5 | 5.012 | 2.796 | 0.039 |
| 13 | 10 | 10 | 10 | 6 | 4.145 | 2.766 | 0.041 |
| 14 | 10 | 15 | 15 | 4 | 4.001 | 2.729 | 0.033 |
| 15 | 10 | 20 | 5 | 5 | 6.241 | 1.598 | 0.016 |
| 16 | 12 | 10 | 15 | 5 | 4.001 | 3.341 | 0.032 |
| 17 | 12 | 15 | 5 | 6 | 5.551 | 3.887 | 0.035 |
| 18 | 12 | 20 | 10 | 4 | 3.998 | 2.512 | 0.034 |

experiments are performed on die sinking EDM machine of FORMATICS 50 model integrated with ELECTRONICA PRS 20. Before machining, the surfaces of electrodes and workpieces are polished and cleaned. In Table 4, the selected input factors and corresponding levels are presented for this investigation. In Table 5, the chosen conditions of experiments are shown. By using the tester of Talysurf, the SR on the machined surfaces is computed. In the transverse direction, the measurements of roughness have been performed with cut-off length of 0.8 mm. The process is repeated for three times, and average values are estimated. Figure 5 illustrates the workpiece images after experimentation.

## 5 Results and discussion

This section describes the experimental results and discussion on PM-EDM of Nimonic alloy 901 workpieces with Cu–W electrode using SiC as a powder particle.

### 5.1 Computation of SR, MRR and TWR

The values of SR can be obtained by calculating the mean absolute deviation from the average surface level; the value

**Table 8** Response table for $S/N$ ratios of SR

| Level | $C_p$ | $T_{on}$ | $I_p$ | $V_s$ |
|---|---|---|---|---|
| 1 | −10.913 | −8.840 | −9.361 | −9.704 |
| 2 | −10.426 | −9.929 | −8.289 | −8.598 |
| 3 | −9.962 | −10.176 | −11.296 | −10.644 |
| 4 | −9.291 | – | – | – |
| 5 | −7.210 | – | – | – |
| 6 | −10.090 | – | – | – |
| Delta | 3.704 | 1.336 | 3.007 | 2.045 |
| Rank | 1 | 4 | 2 | 3 |

of surface finish is retrieved based on a tester of computer-controlled SR. The values of MRR and TWR can be computed using Eqs. (2), and (3), respectively.

### 5.2 $S/N$ ratio for response characteristics

The output-influenced parameters can be classified as two classes such as controllable, i.e. design parameters, and uncontrollable, i.e. noise parameters. Usually, the factors whose values can be adjusted and easily set out by the designer are said to be controllable while the uncontrollable
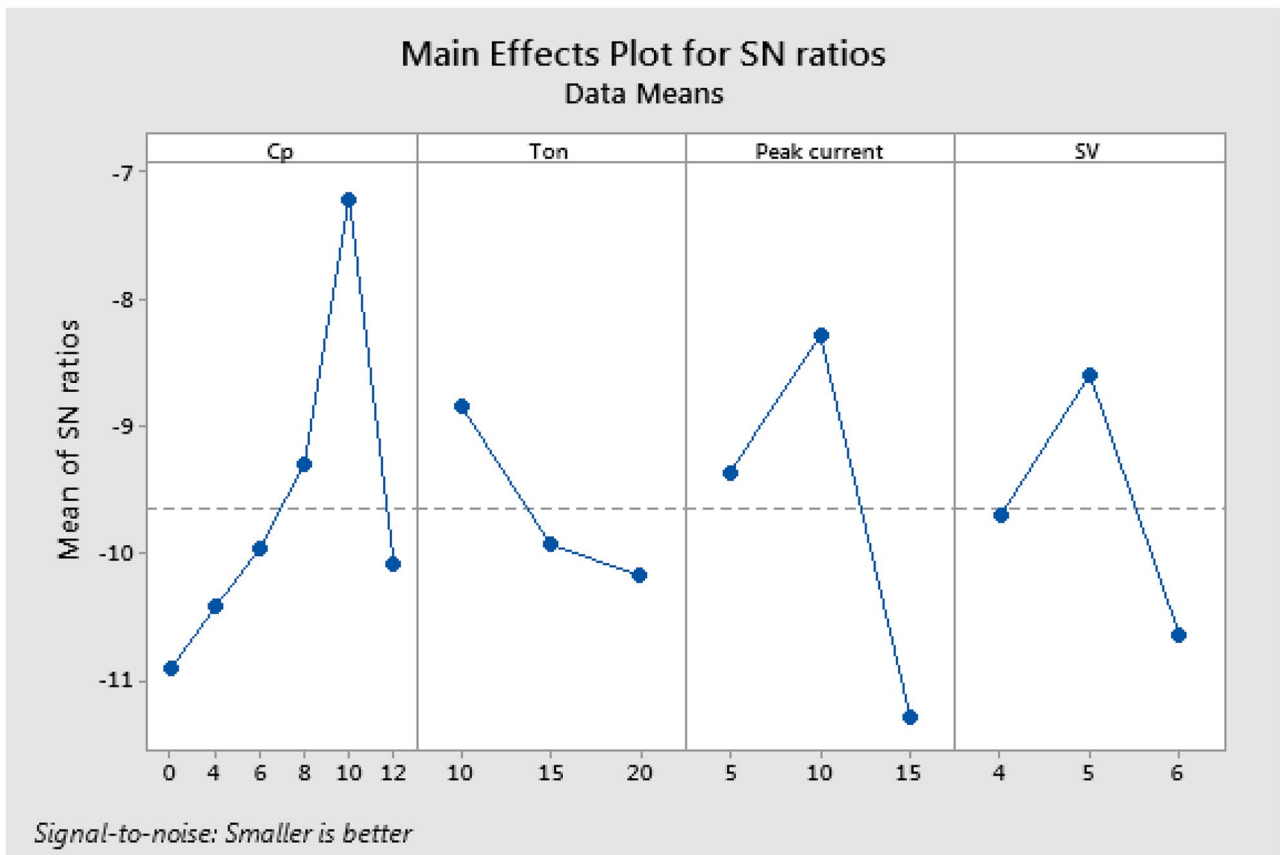


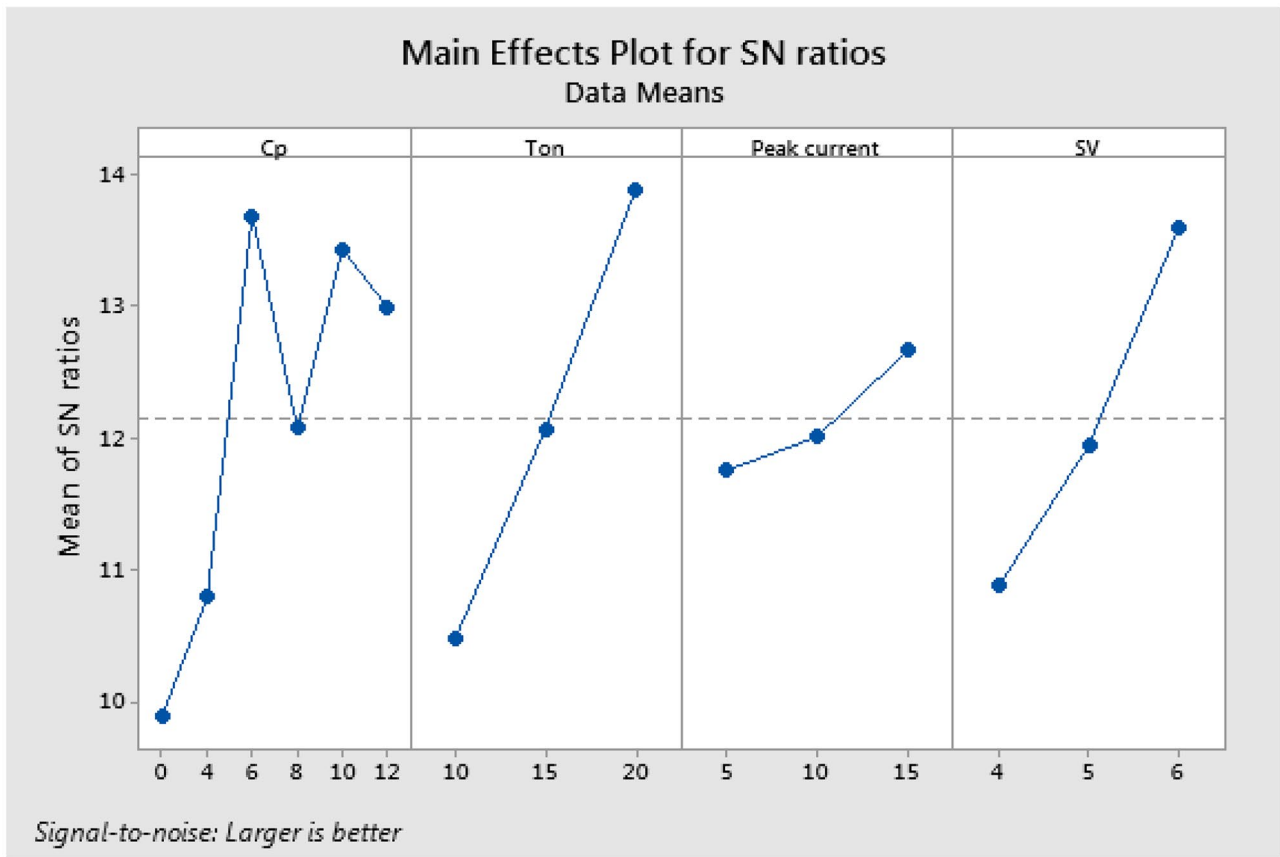**Fig. 6** The main effect plot for $S/N$ ratios of SR

**Fig. 7** The main effect plot for MRR $S/N$ ratios

parameters are the variation of sources associated with operational environment. Based on the conducted experiments, the control factors with the best settings are estimated as they influence the output parameters. The below-mentioned different types of $S/N$ ratios like higher-lower-the-better (LB) and the-better (HB) are incorporated by relying on the response type. Table 6 lists the criteria considered in this work while Table 7 illustrates the obtained values of output responses such as MRR, SR and TWR:

$$(S/N)HB = -10 \ log \ (MSD_{HB}) \tag{4}$$

where the mean square deviation (MSD) for HB response is computed as follows:

$$MSD_{HB} = \frac{1}{R}\sum_{i=1}^{R}\left(\frac{1}{Y_i}\right)^2 \tag{5}$$

$$(S/N) \ LB = -10 \ log \ (MSD_{LB}) \tag{6}$$

**Table 9** The values of response for $S/N$ ratios (MRR)

| Level | $C_p$ | $T_{on}$ | $I_p$ | $V_s$ |
|-------|-------|----------|-------|-------|
| 1 | 9.885 | 10.475 | 11.753 | 10.876 |
| 2 | 10.788 | 12.069 | 12.008 | 11.945 |
| 3 | 13.688 | 13.883 | 12.666 | 13.606 |
| 4 | 12.072 | – | – | – |
| 5 | 13.433 | – | – | – |
| 6 | 12.989 | – | – | – |
| Delta | 3.803 | 3.408 | 0.913 | 2.731 |
| Rank | 1 | 2 | 4 | 3 |

**Table 10** The values of response for $S/N$ ratios of TWR

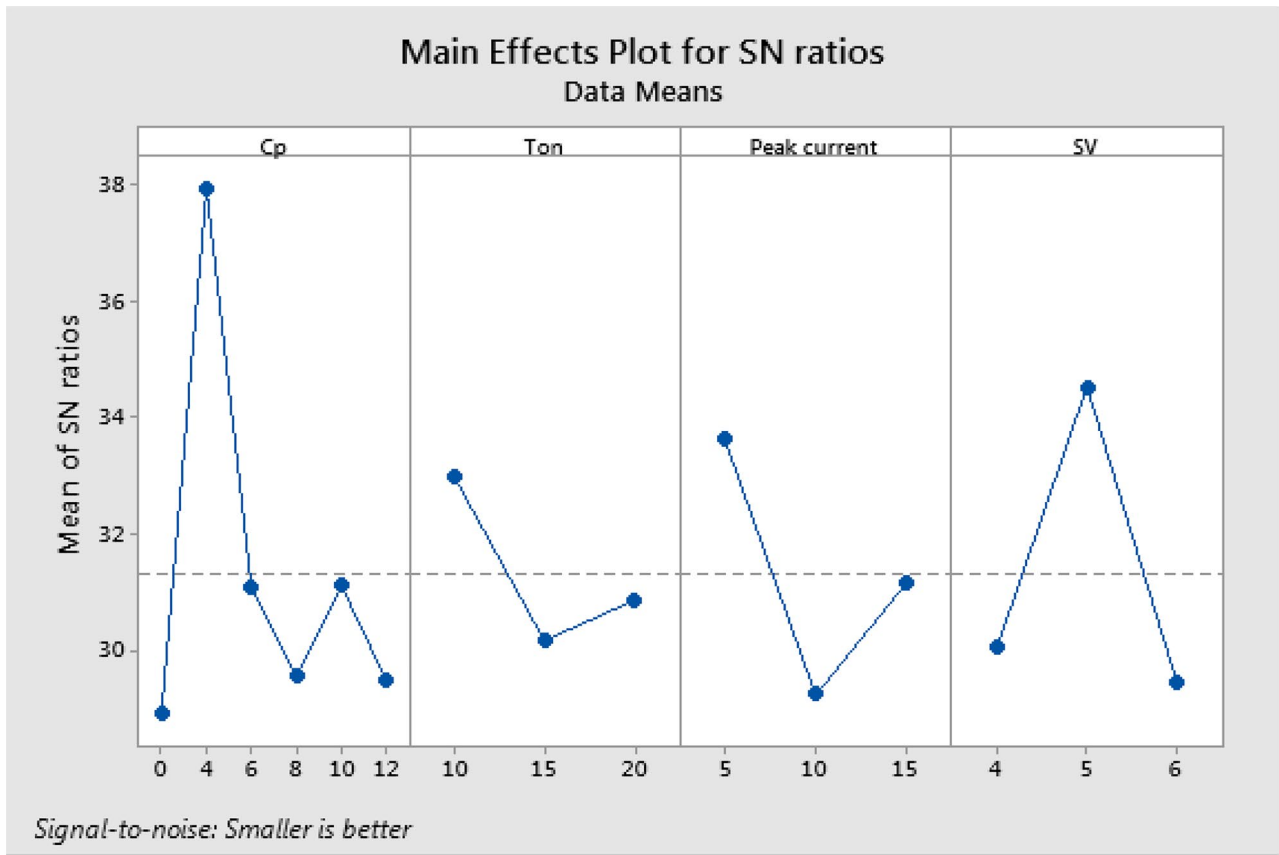| Level | $C_p$ | $T_{on}$ | $I_p$ | $V_s$ |
|-------|-------|----------|-------|-------|
| 1 | 28.90 | 32.98 | 33.62 | 30.04 |
| 2 | 37.93 | 30.16 | 29.22 | 34.52 |
| 3 | 31.06 | 30.85 | 31.15 | 29.43 |
| 4 | 29.54 | – | – | – |
| 5 | 31.10 | – | – | – |
| 6 | 29.46 | – | – | – |
| Delta | 9.02 | 2.82 | 4.39 | 5.09 |
| Rank | 1 | 4 | 3 | 2 |

**Fig. 8** The main effect plot for TWR $S/N$ ratios

where the mean square deviation (MSD) for LB response is computed as follows:

$$MSD_{LB} = \frac{1}{R}\sum_{i=1}^{R}\left(Y_i\right)^2 \qquad (7)$$

As shown in Fig. 6 (the effect on SR), the higher impact on process factors of performance measures is shown by the response line deviation in regard to the horizontal line. In PM-EDM, the most significant machining parameters are $C_p$ and $I_p$ for SR followed by $V_s$ and $T_{on}$ to machine the Cu–W electrode–based Nimonic alloy 901. In Table 8, the SR measurements are shown derived from the $S/N$ ratio values and the experiments. As shown in Fig. 7 (the effect on MRR),

the higher impact on process factors of performance measures is shown by the response line deviation in regard to the horizontal line. In PM-EDM, the most significant machining parameters are $C_p$ and $T_{on}$ for MRR followed by $I_p$ and $V_s$ to machine the Cu–W electrode–based Nimonic alloy 901. The values of MRR measured from the experiments and their corresponding values of $S/N$ ratios are listed in Table 9.

As shown in Fig. 8 (the effect on TWR), the higher impact on process factors of performance measures is shown by the response line deviation in regard to the horizontal line. In PM-EDM, the most significant machining parameters are $C_p$ and $V_s$ for TWR followed by $I_p$ and $T_{on}$ to machine the Cu–W electrode–based Nimonic alloy 901. The values of

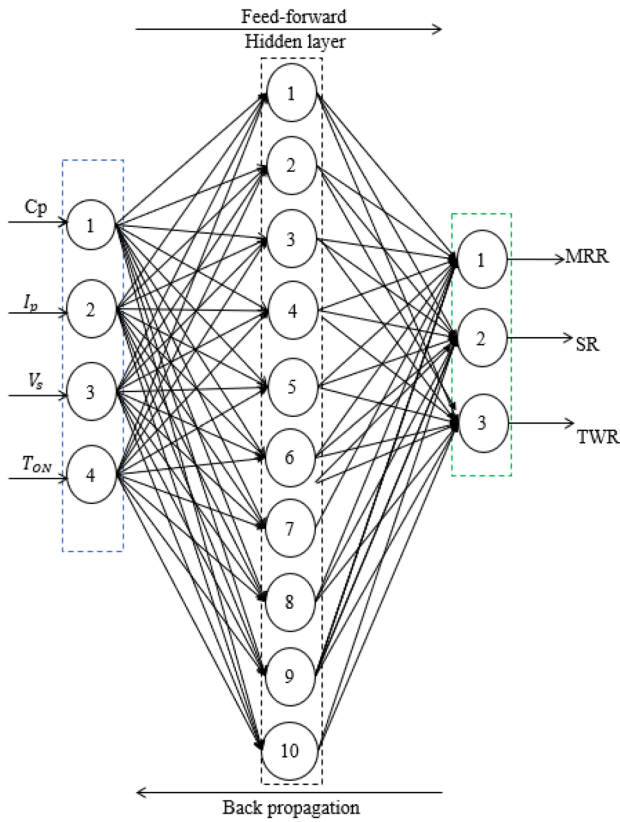**Fig. 9** Block diagram of proposed FF-BPNN with scalable conjugate gradient
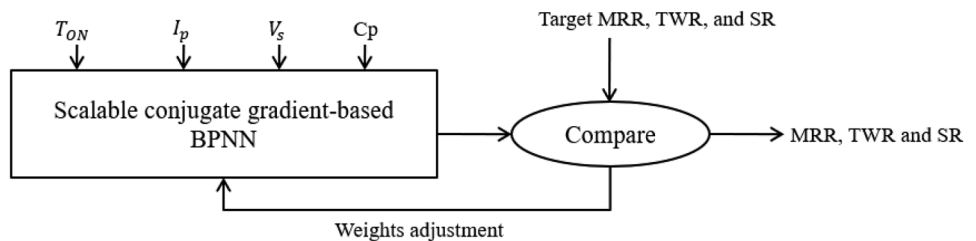
**Fig. 10** Neural network model of the proposed FF-BPNN (4–10-3) architecture

TWR measured from experiments and their corresponding values of $S/N$ ratios are listed in Table 10.

## 5.3 Proposed FF-BPNN modelling

The proposed scalable conjugate gradient-with FF-BPNN block diagram is presented in Fig. 9, in which input process parameters such as Cp, $I_p$, $V_s$ and $T_{on}$ are fed into the proposed 4–10-3 architecture of FF-BPNN. Furthermore, this network consists of an output layer, single input layer and hidden layer as shown in Fig. 10. The input layer has four nodes that represent the input nodes, which are used to hold the data from Cp, $I_p$, $V_s$ and $T_{on}$. The hidden layer has ten nodes labelled as hidden nodes, while the output layer has three nodes labelled as output nodes: MRR, TWR and SR. The proposed PM-EDM process modelling involves two phases: network training and testing of experimental machining data.

Here, the training dataset holds the information of $T_{on}$, $I$, $V_s$, Cp, TWR, SR and MRR. The anticipated MRR, TWR and SR are compared to the E-MRR-, E-SR- and E-TWR-based target values. The weight adjustment will be utilized to compute the final optimized levels of P-MRR, P-SR and P-TWR, which will lower the error values.

### 5.3.1 Data preprocessing

Prior to training the NN and learning mapping, it is critical to convert the experimental data into patterns. Create training or testing pattern vectors, each of which is made up of an input condition vector $P_i$, which contains Cp, $T$, $I$ and $V_S$, and a target vector $T_i$, which contains MRR and Ra. In the case of multiple operating ranges for process parameters, it is critical to consider the input and output data scale. The ANN will be efficiently trained without

**Table 11** Obtained values of output response parameters using experimental and FF-BPNN model

| S. No | $C_p$ | $T_{on}$ | $I_p$ | $V_s$ | E-MRR | P-MRR | E-SR | P-SR | E-TWR | P-TWR |
|-------|-------|----------|-------|-------|-------|-------|------|------|-------|-------|
| 1 | 0 | 10 | 5 | 4 | 2.241 | 2.235 | 3.123 | 3.115 | 0.04 | 0.039 |
| 2 | 0 | 15 | 10 | 5 | 2.713 | 2.699 | 2.546 | 2.541 | 0.035 | 0.034 |
| 3 | 0 | 20 | 15 | 6 | 4.998 | 4.887 | 5.452 | 5.442 | 0.033 | 0.0331 |
| 4 | 4 | 10 | 5 | 5 | 2.321 | 2.311 | 2.652 | 2.651 | 0.03 | 0.031 |
| 5 | 4 | 15 | 10 | 6 | 4.459 | 4.462 | 2.761 | 2.764 | 0.031 | 0.0311 |
| 6 | 4 | 20 | 15 | 4 | 4.012 | 4.011 | 5.003 | 5.001 | 0.022 | 0.0219 |
| 7 | 6 | 10 | 10 | 4 | 3.985 | 3.875 | 2.245 | 2.241 | 0.029 | 0.0291 |
| 8 | 6 | 15 | 15 | 5 | 4.864 | 4.86 | 3.768 | 3.761 | 0.021 | 0.0211 |
| 9 | 6 | 20 | 5 | 6 | 5.831 | 5.831 | 3.690 | 3.691 | 0.036 | 0.0361 |
| 10 | 8 | 10 | 15 | 6 | 4.039 | 4.032 | 2.612 | 2.619 | 0.028 | 0.0281 |
| 11 | 8 | 15 | 5 | 4 | 3.195 | 3.184 | 3.389 | 3.381 | 0.034 | 0.0341 |
| 12 | 8 | 20 | 10 | 5 | 5.012 | 5.011 | 2.796 | 2.786 | 0.039 | 0.0389 |
| 13 | 10 | 10 | 10 | 6 | 4.145 | 4.141 | 2.766 | 2.754 | 0.041 | 0.0401 |
| 14 | 10 | 15 | 15 | 4 | 4.001 | 4.004 | 2.729 | 4.003 | 0.033 | 0.0319 |
| 15 | 10 | 20 | 5 | 5 | 6.241 | 6.232 | 1.598 | 1.589 | 0.016 | 0.0162 |
| 16 | 12 | 10 | 15 | 5 | 4.001 | 4.004 | 3.341 | 3.339 | 0.032 | 0.0319 |
| 17 | 12 | 15 | 5 | 6 | 5.551 | 5.555 | 3.887 | 3.879 | 0.035 | 0.0348 |
| 18 | 12 | 20 | 10 | 4 | 3.998 | 3.996 | 2.512 | 2.499 | 0.034 | 0.0341 |

**Fig. 11** Performance comparison of E-MRR obtained using experimentation and P-MRR obtained using FF-BPNN model
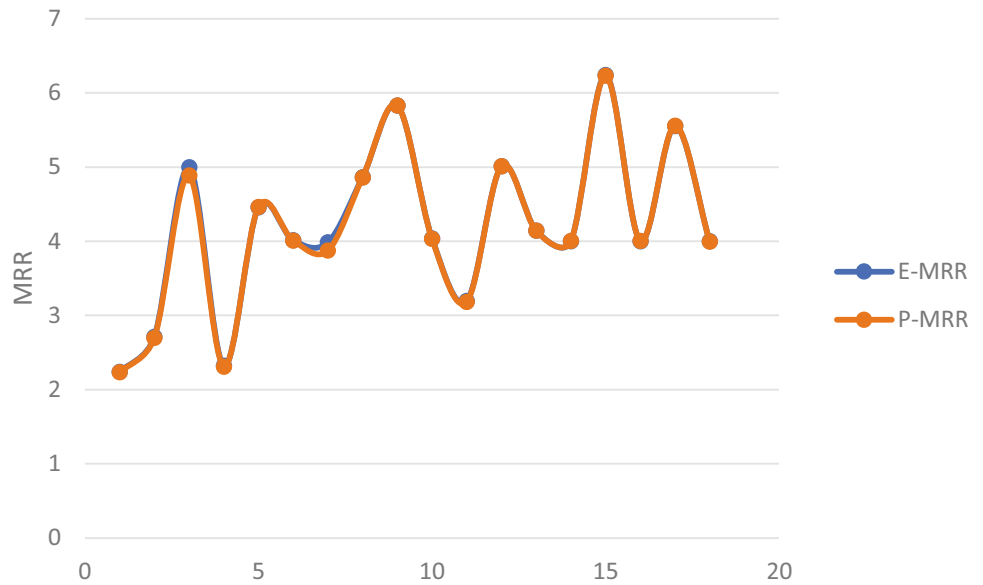


any skewing variable results by ensuring the scaling or normalization. All input parameters are equally essential in the training, and each term is mapped to a value between −1 and 1 using the formula below:

$$N = \frac{(R - R_{\min}) \times (N_{\max} - N_{\min})}{(R_{\max} - R_{\min})} + N_{\min} \qquad (6)$$

The normalized value of the real variable is indicated by $N$, and its maximum and minimum values are denoted as $N_{\min}$ and $N_{\max}$, respectively. Here, real variable is denoted by $R$ with its maximum and minimum values denoted by $R_{\max}$ and $R_{\min}$, respectively. Table 11 shows the comparison of MRR, TWR and SR output responses derived by experimental and prediction, indicated as P-MRR, P-SR and P-TWR. Figures 11, 12 and 13 show

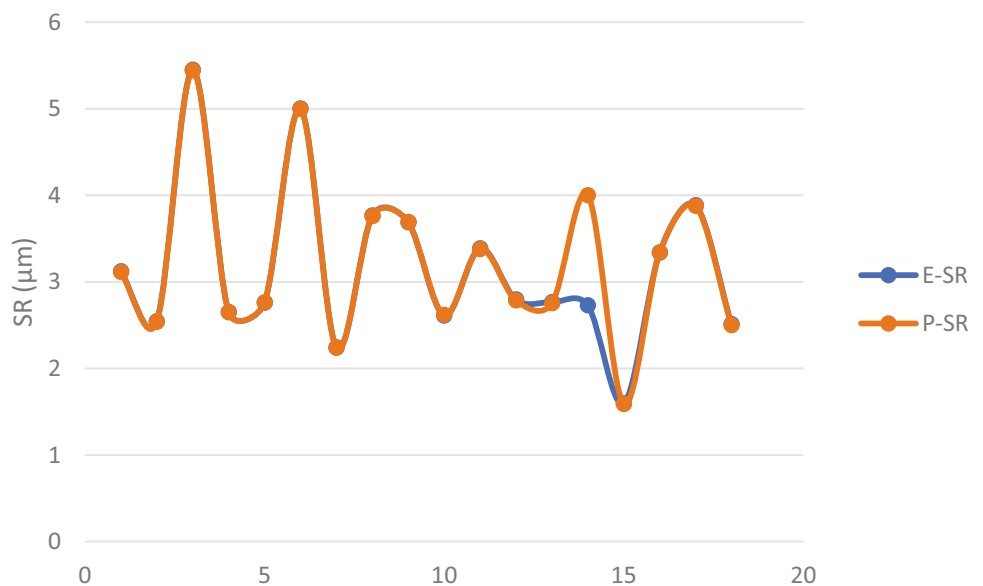**Fig. 12** Comparison of obtained SR values using experimentation and FF-BPNN model

**Fig. 13** Comparison of obtained TWR values using experimentation and FF-BPNN model
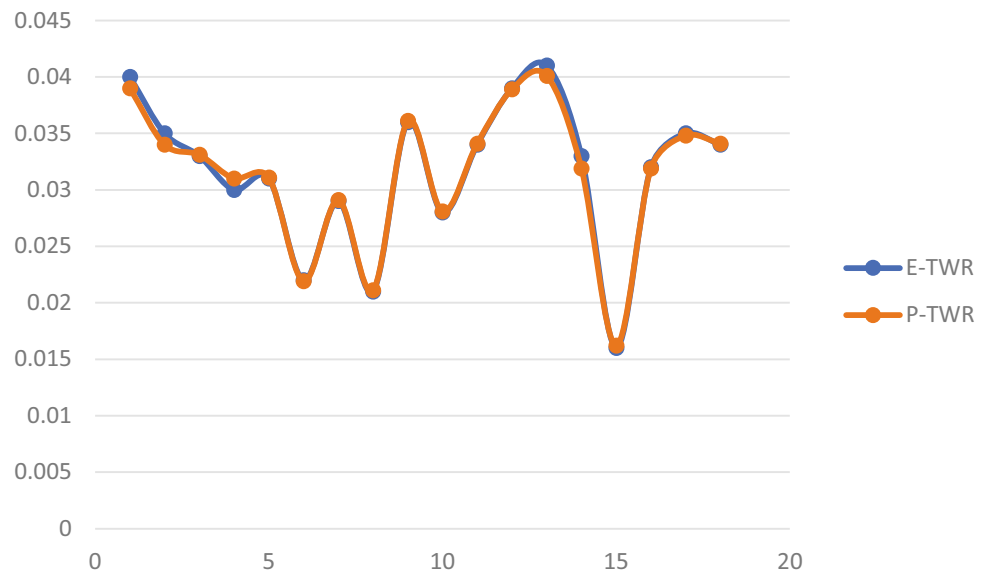


**Table 12** Final optimization results of PM-EDM process in different machining regimes

| Setting level | Optimal TWR, SR and MRR parameters | | | | | |
|---|---|---|---|---|---|---|
| | E-MRR | P-MRR | E-SR | P-SR | E-TWR | P-TWR |
| $C_p$-10%, $T_{on}$-20, $I_p$-5 and $V_s$-5 | 6.241 | 6.232 | 1.598 | 1.589 | 0.016 | 0.0162 |
| Relative error (in %) | 0.14 | | 0.56 | | 1.234 | |

the performance comparison graph of the obtained values of E-MRR, P-MRR, E-SR and P-SR and E-TWR and P-TWR, respectively. Table 12 shows the final confirmation test findings.

# 6 Conclusion

Powder mixing into the EDM's dielectric fluid is a modern evolution to ensure the better rates of machining at reduced TWR with the desired surface quality. Based on the main and trial experiments, the proposed investigation on PM-EDM of Nimonic alloy 901 resulted in the minimum TWR and higher MRR in addition to the powder concentration in EDM oil. The current studies obtained the results to choose the optimum conditions of machining the workpiece made of Nimonic alloy 901, which has been widely utilized in exhaust system of formula one car, rocket engine and steam turbine. The experimental results have drawn the below-mentioned conclusions within the range of chosen parameters.

- The maximum values of MRR and the minimal values of SR and TWR are obtained at $I_p$ of 5A, 5 V of $V_s$, a moderate $T_{on}$ as 20 μs, and $C_p$ of 10%.

- Confirmation test results demonstrated that the relative error is less than 1.5% for SR, MRR and TWR.

We confirm that the manuscript is the authors' original work, and the manuscript has not received prior publication and is not under consideration for publication elsewhere. On behalf of all the co-authors, we shall bear full responsibility for the submission. We declare that I shall not submit the paper for publication in any other journal till the decision is made by journal editors.

**Author contribution** **Author 1: Ravi Varma Penmetsa**, Conceived and design the analysis, Collecting the data, Wrote the paper. **Author 2: Ashok Kumar Ilanko**, Contributed data and analysis tools. **Author 3: Siriyal Rajesh**, Performed the analysis. **Author 4: Rama Bhadri Raju Chekuri**, Manuscript editing and figure design.

## Declarations

# References

1. Khan MY, Rao PS (2019) Electrical discharge machining: vital to manufacturing industries, International Journal of Innovative Technology and Exploring. Engineering 8(11):1696–1701

2. Amorim FL, Weingaertner WL (2004) Die-sinking electrical discharge machining of a high-strength copper based alloy for injection molds. J Braz Soc Mech Sci Eng 26(2):137–144

3. Patel MR, Barrufet MA, Eubank PT, DiBitonto DD (1989) Theoretical models of the electrical discharge machining process. II. The anode erosion model. J Appl Phys 66(9):4104–4111

4. El-Hofy HA (2005) Advanced machining processes: nontraditional and hybrid machining processes. McGraw Hill Professional

5. Chekuri RBR, Kalluri R, Rajesh S, Palakollu JK (2017) A study on die sinking EDM of Nimonic C-263 super alloy: modelling and optimization. J Adv Res Dyn Control Sys 9(17):2120–2130

6. Rao PS, Jain PK, Dwivedi DK (2015) Electro chemical honing (ECH) of external cylindrical surfaces of titanium alloys. Procedia Eng 100:936–945

7. Chekuri RBR, Kalluri R, Palakollu JK, Rajesh S (2019) Modelling and optimization of machining high-performance nickel based super alloy Nimonic C-263 using die sinking EDM. Int J Mech Eng Robot Res 8(2):196–201

8. Chakraborty S, Kar S, Dey V, Ghosh SK (2018) The phenomenon of surface modification by electro-discharge coating process: a review. Surf Rev Lett 25(1). https://doi.org/10.1142/S0218625X18300034

9. Kumar A, Maheshwari S, Sharma C, Beri N (2010) Research developments in additives mixed electrical discharge machining (AEDM): a state of art review. Mater Manuf Process 25(10):1166–1180

10. Beri N, Maheshwari S, Sharma C, Kumar A (2010) Technological advancement in electrical discharge machining with powder metallurgy processed electrodes: a review. Mater Manuf Process 25(10):1186–1197

11. Zhao WS, Meng QG, Wang ZL (2002) The application on research of powder mixed EDM in rough machining. J Mater Process Technol 129(1–3):30–33

12. Lu ZZ, Zhao FL, Yang YY (2008) Research on dielectric breakdown and discharge channel in powder-mixed EDM. Dalian Ligong DaxueXuebao/Journal of Dalian University of Technology 48(3):373–377

13. Talla G, Gangopadhayay S, Biswas CK (2016) State of art in powder-mixed electric discharge machining: a review. Proceedings of the Institution of Mechanical Engineers, Part B: Journal of Engineering Manufacture 231(4):2511–2526

14. Prihandana GS, Mahardika M, Hamdi M, Wong YS, Mitsui K (2011) Accuracy improvement in nanographite powder-suspended dielectric fluid for micro-electrical discharge machining processes. Int J Adv Manuf Technol 56:143–149

15. Xin B, Gao M, Li S, Feng B (2020) Modeling of interelectrode gap in electric discharge machining and minimum variance self-tuning control of interelectrode gap. Math Probl Eng 2020:5652197. https://doi.org/10.1155/2020/5652197

16. Chow HM, Yang LD, Lin CT, Chen YF (2008) The use of SiC powder in water as dielectric for micro-slit EDM machining. J Mater Proc Technol 195(1–3):160–170

17. Kung KY, Horng JT, Chiang KT (2009) Material removal rate and electrode wear ratio study on the powder mixed electrical discharge machining of cobalt-bonded tungsten carbide. Int J Adv Manuf Tech 40:95–104

18. Jahan MP, Rahman M, Wong YS (2010) Modelling and experimental investigation on the effect of nano powder mixed dielectric in micro-electro discharge machining of tungsten carbide. Proc Inst Mech Eng B J Eng Manuf 224:1725–1739

19. Gosai ND, Joshi AY (2016) Experimental investigation and optimization of process parameters used in the silicon powder mixed electro discharge machining of Ti-6Al-4V alloy using response surface methodology. J Manuf Sci Prod 16(1):21–32

20. Tripathy S, Tripathy DK (2016) Multi-attribute optimization of machining process parameters in powder mixed electro-discharge machining using TOPSIS and grey relational analysis. Eng Sci Technol Int J 19(1):62–70

21. Gugulothu B, Rao DH, Rao GKM (2015) Optimization of EDM process parameters and graphite powder concentration on electrical discharge machining of Ti-6al-4v alloy using Taguchi method. Int J Adv Prod Mech Eng 1(5):31–44

22. Kolli M, Kumar A (2015) Effect of dielectric fluid with surfactant and graphite powder on electrical discharge machining of titanium alloy using Taguchi method. Eng Sci Technol Int J 18(4):524–535

23. Kuriachen B, Mathew J (2016) Effect of powder mixed dielectric on material removal and surface modification in micro electric discharge machining of Ti-6Al-4V. Mater Manuf Processes 31(4):439–446

24. Singh B, Kumar J, Kumar S (2016) Investigation of the tool wear rate in tungsten powder mixed electric discharge machining of AA6061/10%SiCp Composite. Mater Manuf Processes 31(4):456–466

25. Surekha B, Lakshmi TS, Jena H, Samal P (2019) Response surface modelling and application of fuzzy grey relational analysis to optimize the multi-response characteristics of EN-19 machined using powder mixed EDM. Aust J Mech Eng 19(1):19–29

26. Opoz TT, Yasar H, Ekmekc N, Ekmekci B (2018) Particle migration and surface modification on Ti6Al4V in SiC powder mixed electrical discharge machining. J Manuf Process 31:744–758

27. Selvarajan L, Rajavel J, Prabakaran V, Sivakumar B, Jeeva G (2018) A review paper on EDM parameter of composite material and industrial demand material machining. Materials Today: Proceedings 5(2):5506–5513

28. Choudhury SD, Sahari NJ, Surekha B, Mondal G (2018) Study on the influence of hybridized powder mixed dielectric in electric discharge machining of alloy steels. Materials Today: Proceedings 5(9):18410–18415

29. Singh G, Singh G, Singh K, Singlad A (2017) Experimental studies on material removal rate, tool wear rate and surface properties of machined surface by powder mixed electric discharge machining. Materials Today: Proceedings 4:1065–1073

30. Chaudhury P, Samantaray S, Sahu S (2017) Multi response optimization of powder additive mixed electrical discharge machining by taguchi analysis. Materials Today: Proceedings 4:2231–2241

31. Daneshmand S, Masoudi B, Monfared V (2017) Electrical discharge machining of Al/7.5% Al2O3 MMCs using rotary tool and Al2O3 powder. Surf Rev Lett 24(2):1750018

32. Panda BK, Kumar S (2019) Impact of powder-mixed electrical discharge machining on surface hardness of AISI D3 Die Steel, 2019 IEEE 10th International Conference on Mechanical and Aerospace Engineering (ICMAE) 218–222. https://doi.org/10.1109/ICMAE.2019.8880966.

33. Joshi AY, Joshi AY (2019) A systematic review on powder mixed electrical discharge machining. Heliyon 5(12):e02963. https://doi.org/10.1016/j.heliyon.2019.e02963

34. Khan MY, Rao PS, Pabla BS (2020) Powder mixed electrical discharge machining (PM-EDM): A methodological review. Material Today: proceedings. https://doi.org/10.1016/j.matpr.2020.10.122

35. Ilani MA, Khoshnevisan M (2020) Powder mixed-electrical discharge machining (EDM) with the electrode is made by fused deposition modeling (FDM) at Ti-6Al-4V machining procedure. Multiscale and Multidiscip. Model Exp Des 3:173–186. https://doi.org/10.1007/s41939-020-00070-6

36. Upadhyay A, Sharma V (2018) Optimizing material removal rate using artificial neural network for micro-EDM. Design and

Optimization of Mechanical Engineering Products 209–233. https://doi.org/10.4018/978-1-5225-3401-3.ch011

37. Payal H, Maheswari S, Bharti PS (2017) Process modelling of electric discharge machining of Inconel 825 using artificial neural networks. Int J Mech Mechatron Eng 11(3):562–566

38. Quarto M, D'Urso G, Giardini C, Maccarini G, Carminati M (2021) A comparison between finite element model (fem) simulation and an integrated artificial neural network (ANN)-particle swarm optimization (PSO) approach to forecast performances of micro electro discharge machining (micro-EDM) drilling. Micromachines 12(6):667. https://doi.org/10.3390/mi12060667

39. Chekuri RBR, Eshwar D, Kotteda TK, Srikanth Varma RS (2022) Experimental and thermal investigation on die-sinking EDM using FEM and multi-objective optimization using WOA-CS 50:101860. https://doi.org/10.1016/j.seta.2021.101860

**Publisher's Note** Springer Nature remains neutral with regard to jurisdictional claims in published maps and institutional affiliations.